

# Wave-function Visualization of Core-induced Interaction of Non-hydrogenic Rydberg Atom in Electric Field

W. Gao,<sup>1,2</sup> M. Deng,<sup>3</sup> H. Cheng,<sup>1,2</sup> S. S. Zhang,<sup>1,2</sup> and H. P. Liu<sup>\*1,2</sup>

<sup>1</sup>*State Key Laboratory of Magnetic Resonance and Atomic and Molecular Physics,  
Wuhan Institute of Physics and Mathematics,  
Chinese Academy of Sciences, Wuhan 430071, People's Republic of China*

<sup>2</sup>*University of Chinese Academy of Sciences, Beijing 100049, People's Republic of China*

<sup>3</sup>*State Key Laboratory of Low-Dimensional Quantum Physics,  
Department of Physics, Tsinghua University, Beijing 100084, China*

(Dated: October 12, 2018)

## Abstract

We have investigated the wave-function feature of Rydberg sodium in a uniform electric field and found that the core-induced interaction of non-hydrogenic atom in electric field can be directly visualized in the wave-function. As is well known, the hydrogen atom in electric field can be separated in parabolic coordinates  $(\eta, \xi)$ , whose eigen-function can show a clear pattern towards negative and positive directions corresponding to the so-called red and blue states without ambiguity, respectively. It can be served as a complete orthogonal basis set to study the core-induced interaction of non-hydrogenic atom in electric field. Owing to complete different patterns of the probability distribution for red and blue states, the interaction can be visualized in the wave-function directly via superposition. Moreover, the constructive and destructive interferences between red and blue states are also observed in the wave-function, explicitly explaining the experimental measurement for the spectral oscillator strength.

PACS numbers: 32.60.+i, 32.70.cs, 32.80.Fb

## I. INTRODUCTION

Ever since the pioneering work on the stark spectra of alkali-metal atoms made by Zimmerman et al in [1], the effect of electric field on non-hydrogenic atoms in Rydberg states has been investigated extensively both theoretically and experimentally [2–5]. In zero field, the difference between hydrogen and non-hydrogenic atoms is reflected by the large quantum defect values embodying core effect for low angular momentum states. When the non-hydrogenic atom is placed in a uniform electric field, this impure Coulomb potential couples levels from different principal quantum number  $n$ , resulting in different ionization mechanism [6, 7]. Several works have been performed to explore the non-hydrogenic behaviour.

Stark map, plotting the level splitting of Rydberg atoms against the increasing electric field strength, is a very direct and popular way to reveal the anticrossing behaviour of non-hydrogenic atoms in electric field. Many theoretical approaches have been developed to deal with Rydberg atoms in electric field. For instance, explicit expressions of the perturbation theory up to seventh order was presented by Silverstone in [8], which is very accurate and effective in obtaining the hydrogenic stark levels. Derived from the Gutzwiller trace formula, the closed-orbit theory was used to calculate photoabsorption cross sections of hydrogen and sodium in a strong electric field [9, 10]. Theoretical work with WKB theory was also conducted in Ref. [2], which basically repro-

duced the photoionization cross sections of the excited  $3^2P_{3/2}$  state of sodium. When the influence of external fields strongly dominates over the core potential, quantum calculations based on finite basis expansion are usually employed for more accurate results. Diverse basis sets have been adopted, including B-splines basis [11], Sturmian basis [12], potential model basis [13] and quantum defect orbital [14].

Among these theoretical methods, the most interesting is the closed-orbit theory closely connecting the photoabsorption spectra and classical orbits, which provides an intuitive and visual physical picture for the non-hydrogenic behaviour. The so-called scaled-energy spectroscopy interpreted the non-hydrogenic lithium stark effect in the term of combined orbits indicating core scattering from one closed orbit to another one [4]. West *et al.* also calculated and animated the field-induced dynamics with classical atomic models for circular states [5]. Their numerical simulations of a classical electron trajectory showed stark oscillations in a dc electric field. For a pure Coulomb potential, the electron backscatters in the linear orbit and nearly retraces the original trajectory in the opposite direction, but for the trajectory in the sodium model potential, a precession of the highly eccentric orbit is found.

More recently, motivated by theoretical predictions of ‘photoionization microscopy’ [15, 16], Stodolna *et al.* made the first direct visual observation of the nodal structure of stark states for hydrogen [17] with the help of photoelectron imaging [18] and an electrostatic zoom lens [19]. The observed interference pattern clearly revealed that the number of dark fringes corresponds to the parabolic number  $n_1$  of the excited quasibound atomic state. It was also visualized previously in the frame-

---

\*E-mail: liuhongping@wipm.ac.cn

works of both a semiclassical open-orbit theory and a quantum-mechanical theory developed by Zhao and Delos in [20, 21]. Based upon Harmin’s semiclassical theory [2, 22], Robicheaux and Shaw calculated the wavepacket dynamics of a Rydberg electron in a strong electric field for rubidium [23]. Different from the WKB approximation, the coupled-channel theory was also developed to stimulate experimental observations for non-hydrogenic atoms [24]. Subsequently, experimental results performed on helium [25] indirectly visualized the coupling between red and blue stark states with the aid of the interference narrowing [26].

The visualization of the wavefunction as well as the coupling between red and blue states is based on a unique feature of hydrogen atom that the Hamiltonian in a static field is separable in terms of the parabolic coordinates  $\eta, \xi$  ( $\eta = r - z, \xi = r + z$ ) and can be strictly solved. Since the parabolic separation for hydrogen in electric field can supply a set of ‘orthogonal’ basis {red states, blue states}, can we reveal the non-hydrogenic effects directly from the eigen-wavefunctions of nonhydrogenic atom in electric fields? In this paper, we will investigate whether the rigorous hydrogenic parabolic states can be served as a set of basis in deeper understanding and visualizing complex dynamics of non-hydrogenic atom in electric field. For this purpose, taking the effect of the atomic core on Rydberg electron into account, we computed the oscillator strength and electron probability distributions for hydrogen and sodium. By comparing their electron probability distributions directly, we show that wave-function can be intuitive in understanding the coupling behaviour of non-hydrogenic atom in static electric fields on benefit of the ‘orthogonality’ of red states and blue states. Moreover, the irregular oscillator strength distribution for sodium is analyzed in the perspective of electric-field-induced interference between hydrogenic parabolic states. The analysis is also compared with our experimental spectrum of sodium in electric field of 840V/cm below and above the saddle point  $E_c$ .

## II. THEORETICAL CALCULATION

Since the exact quantum defect theory (EQDT) has been detailed previously [27, 28], only a brief summary is given here. The sodium in a uniform electric field oriented along the  $z$ -axis can be described by an exact non-relativistic Hamiltonian, hereafter in atomic units, taking the form

$$H = \frac{p^2}{2} + V^c(r) + Fz, \quad (1)$$

where  $V^c(r)$  is the Coulomb potential including the effects of core-induced electron screening, leading to non-separable of Hamiltonian in parabolic coordinates. Instead of using the model potential [13] or the R-matrix method [29] including the quantum defects implicitly, we employ an equivalent form for the central field potential

[30, 31]:

$$V(r) = \frac{\lambda(\lambda + 1) - l(l + 1)}{2r^2} - \frac{1}{r}, \quad (2)$$

where  $\lambda = l - \delta + \text{Int}(\delta)$  and the quantum defects are explicitly enclosed. Here  $\text{Int}(\delta)$  is the rounded nearest-integer value of the quantum defect. A reduced quantum defect  $\delta' = \delta - \text{Int}(\delta)$  is employed here to assess the real contribution of the quantum defect for a given angular momentum channel. We will directly use  $\delta$  to stand for  $\delta'$  for abbreviation.

Solving the time-independent Schrödinger equation

$$H\psi = E\psi, \quad (3)$$

we can compute the energy levels and their wavefunctions, from which transition probabilities are calculated.

The radial part of the wavefunction is expanded in the B-spline basis and the angular part in the truncated associated Legendre function basis,

$$\psi(r, \theta) = \sum_{n=0}^{N-1} \sum_{l=|m|}^{l_{\max}} C_{nl} \frac{B_n^k(r)}{r} P_l^{|m|}(\theta), \quad (4)$$

where  $P_l^{|m|}(\theta)$  is the normalized associated Legendre function and  $B_n^k(r)$  the  $k$  order B-spline function defined in Refs.[32, 33].

Substituting the Hamiltonian expressed in Eq.(1) and the wavefunction in Eq.(4) into Eq.(3), the Schrödinger equation is transformed into a general eigenvalue problem,

$$HC = ESC, \quad (5)$$

where  $E$  and  $C$  represent eigenvalues and their corresponding eigenvectors, respectively.  $H$  is the matrix form of the Hamiltonian and  $S$  the overlap matrix. Accurate matrix elements are obtained efficiently through the Gauss-Legendre quadrature scheme. A Lanczos algorithm [34] for the general eigenproblem applied to the matrix equation can give the eigenvalue  $E$  and eigenvector  $C$ , which makes the calculation very effective. The oscillator strength for the one-photon dipole transition from the ground state  $|i\rangle$  to the final state  $|f\rangle$  can be expressed as

$$c_{i \rightarrow f} = |\langle i | d | f \rangle|^2, \quad (6)$$

where  $d$  is the electric dipole operator.

## III. RESULTS AND DISCUSSIONS

To study the visual feature of the wavefunction of atom with core-induced interaction in electric field, we have to choose an appropriate energy range within which the spectrum can be well resolved experimentally, and at the

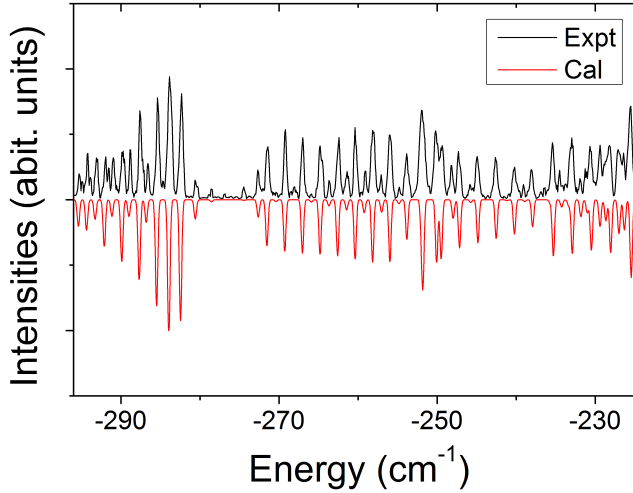


FIG. 1: (Color online) Comparison of the experimental (upper panel) and theoretical (lower panel) stark spectra for Rydberg sodium in the electric field  $F = 840$  V/cm with  $\pi$ -polarized laser irradiation.

time, theoretically, it should be simple enough for the wavefunction analysis.

We experimentally measure the stark spectrum of Rydberg sodium in electric field of 840 V/cm in the energy range  $-290 \text{ cm}^{-1} < E < -230 \text{ cm}^{-1}$  and carry out a theoretical calculation with the present EQDT method. They are shown in Fig.1. In the experiment, the laser is linearly polarized parallel to the electric field  $F$ , thus the  $\Delta m = 0$  transition occurs. In the calculation, we adopt the reduced quantum-defect values from Ref. [1], taking  $\delta_s = 0.347$ ,  $\delta_p = -0.146$  and  $\delta_d = 0.014$ . Quantum defect values for all higher angular momenta are negligibly small and set as zero. The theoretical oscillator strength is convoluted with a Gaussian profile of  $0.18 \text{ cm}^{-1}$  to give a spectrum comparable with experimental observation. The Gaussian broadening includes the Doppler broadening and the laser linewidth. To facilitate a direct comparison, the experimental observation and the convoluted spectrum are shown in mirror fashion. It's obvious that for the current electric field strength and energy range, the experimental resonances are well resolved to be comparable to calculation. Although trivial differences in relative intensities for several resonances exist due to the inhomogeneity in the electric field and instability of the laser power, the agreement between theoretical calculation and experimental observation is rather satisfactory both for the positions and intensities under present condition. This serves as a strong evidence of the validity of EQDT method and supplies a reliable groundwork for the analysis of the oscillator strength re-distribution and wavefunction feature.

In Fig.1, we can also notice that the spectral lines, for example, in the energy range  $-270 \sim -250 \text{ cm}^{-1}$ , are accompanied with some lines with weak intensities. These weak lines are due to the core-induced interaction for sodium in electric field. As a result, the spec-

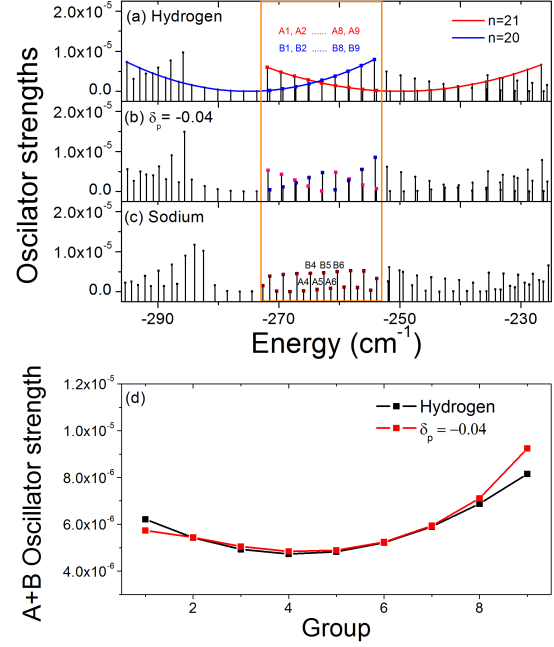


FIG. 2: (Color online) Theoretical calculation of photoexcitation spectrum from the ground state to stark manifolds  $n = 19$  to 23 with laser polarized parallel to the electric field  $F = 840$  V/cm for (a) hydrogen atom, (b) artificial atom with  $\delta_p = -0.04$  and (c) sodium atom, and the oscillator strength sums of the interacting spectral peaks (d). The complete stark manifold of  $n = 20$  (blue dots + line) and  $n = 21$  (red dots + line) of hydrogen in (a) are specially marked out to trace the symmetric envelop and make the crossing characteristic clear. Note that the spectral lines in crossing area are numbered to facilitate the analysis. For the closely interacting pair of peaks for the artificial atom, their oscillator strength sums are kept constant for the first order approximation, compared with hydrogen atom.

tral line intensity re-distribution is an indicator for the non-Coulombic potential interaction. To make it clear, we calculate a series of oscillator strengths for three different atomic systems, from simple to complex, including hydrogen, artificial non-hydrogenic atom and sodium. Specifically, the artificial non-hydrogenic atom has only one quantum defect channel  $\delta_p = -0.04$ , more complex than hydrogen atom but much simpler than the real sodium atom. Sodium atom has non-ignorable quantum defects for  $s$ ,  $p$  and  $d$  channels. We calculate the oscillator strengths for these three types of atoms in the energy range corresponding to that in Fig.1, which is shown in Fig.2. The energy level positions are listed in table I, where we can see that our calculations for hydrogen atom by the EQDT method are exactly the same as that by the seventh-order perturbation theory [8] up to three digital number. Our calculation for sodium by the EQDT method agree with the experimental observation within the Gaussian broadening of  $0.18 \text{ cm}^{-1}$ .

As shown in Fig.2(a), for hydrogen atom, the oscilla-

TABLE I: The energy level positions (in  $\text{cm}^{-1}$ ) of the Stark resonances of hydrogen and sodium ( $F = 840 \text{ V/cm}$ ,  $m = 0$ ) within  $-270 \text{ cm}^{-1} \sim -250 \text{ cm}^{-1}$  shown in Fig.2.

hydrogen			sodium		
State:( $n_1, n_2, m$ )	Theory <sup>a</sup>	Theory <sup>b</sup>	State	Theory <sup>c</sup>	Experiment <sup>d</sup>
(19,0,0)	-254.228	-254.228	A1	-272.628	-272.674
(18,1,0)	-256.393	-256.393	B1	-271.534	-271.403
(17,2,0)	-258.558	-258.558	A2	-270.390	-270.300
(16,3,0)	-260.721	-260.721	B2	-269.276	-269.198
(15,4,0)	-262.882	-262.882	A3	-268.159	-268.011
(14,5,0)	-265.042	-265.042	B3	-267.038	-266.993
(13,6,0)	-267.201	-267.201	A4	-265.922	-265.891
(12,7,0)	-269.359	-269.359	B4	-264.811	-264.788
(11,8,0)	-271.515	-271.515	A5	-263.684	-263.686
(0,20,0)	-271.912	-271.912	B5	-262.588	-262.413
(1,19,0)	-269.666	-269.666	A6	-261.447	-261.395
(2,18,0)	-267.419	-267.419	B6	-260.373	-260.377
(3,17,0)	-265.170	-265.170	A7	-259.220	-259.105
(4,16,0)	-262.919	-262.919	B7	-258.164	-258.172
(5,15,0)	-260.666	-260.666	A8	-257.015	-257.069
(6,14,0)	-258.412	-258.412	B8	-255.972	-256.051
(7,13,0)	-256.156	-256.156	A9	-254.839	-254.778
(8,12,0)	-253.898	-253.898	B9	-253.828	-253.844

<sup>a</sup> Calculation for hydrogen by the seventh-order perturbation theory [8];

<sup>b</sup> Calculation for hydrogen by the present EQDT method, exactly the same as that by the above perturbation theory;

<sup>c</sup> Calculation for sodium by the present EQDT method;

<sup>d</sup> Experimental observation for sodium (laser linewidth is about  $0.09 \text{ cm}^{-1}$  and the total Gaussian broadening is  $0.18 \text{ cm}^{-1}$ ).

tor strength distribution shows high regularity. For the stark manifold belonging to a specified principal quantum number  $n$ , there are two energy levels corresponding to the same  $|n_1 - n_2|$  value, but they have the same oscillator strength. In addition, for a specified  $n$ , the oscillator strengths of a parabolic state will decrease as the value of  $|n_1 - n_2|$  decreases and reach minimum when  $|n_1 - n_2|$  reaches the minimum. Kondratovich and Delos have derived a simple semiclassical formula to interpret the symmetric envelop of a complete stark manifold for the hydrogenic  $m = 0$  case [35]. They considered that the oscillator strength of a parabolic state is proportional to the absolute square of the quantum angular function of the outgoing waves. The most important property of hydrogen atom in electric field is that energy levels belonging to different principal quantum number  $n$  can cross each other without interaction. This unique feature is attributed to the  $\text{SO}(4)$  symmetry of the Coulomb potential of hydrogen [36]. Any deviation from the pure Coulomb potential will break this symmetry and cause the coupling between two hydrogenic energy levels, resulting in irregularity of oscillator strength distribution of non-hydrogenic atoms. This irregularity can be seen from the calculated oscillator strengths for artificial atom and sodium atom, as shown in Fig.2(b) and (c), respec-

tively. For the artificial atom, there is only one channel with quantum defect so that it behaves closer to a hydrogen atom, providing us a theoretical model to investigate the core-induced interaction by spectral splitting and oscillator strength.

Regarding two energy levels close to each other as a group, the sums of the two oscillator strengths for hydrogen and artificial atom are presented in Fig.2(d). The oscillator strengths summed over two coupling hydrogenic parabolic states are almost conserved, specially for the groups with energy levels close each other. Some discrepancies exist for group 1 and 9, which shows more energy levels take part in the interaction at these points. This oscillator strength conservation provides a way to study the core-induced interaction between red and blue states. For the real atom, sodium, the interactions are so strong that the group classification is tricky, as shown in Fig.2(c). In this case, more than two energy levels participate in the interaction at any given energy range within  $-270 \sim -250 \text{ cm}^{-1}$  and it is difficult to group the spectral lines.

Rather than studying the interaction in the point of view of energy level, we can visualize it on the wavefunction directly, which is shown in Fig.3. For hydrogen atom shown in Fig.3(a), the electron probability distri-

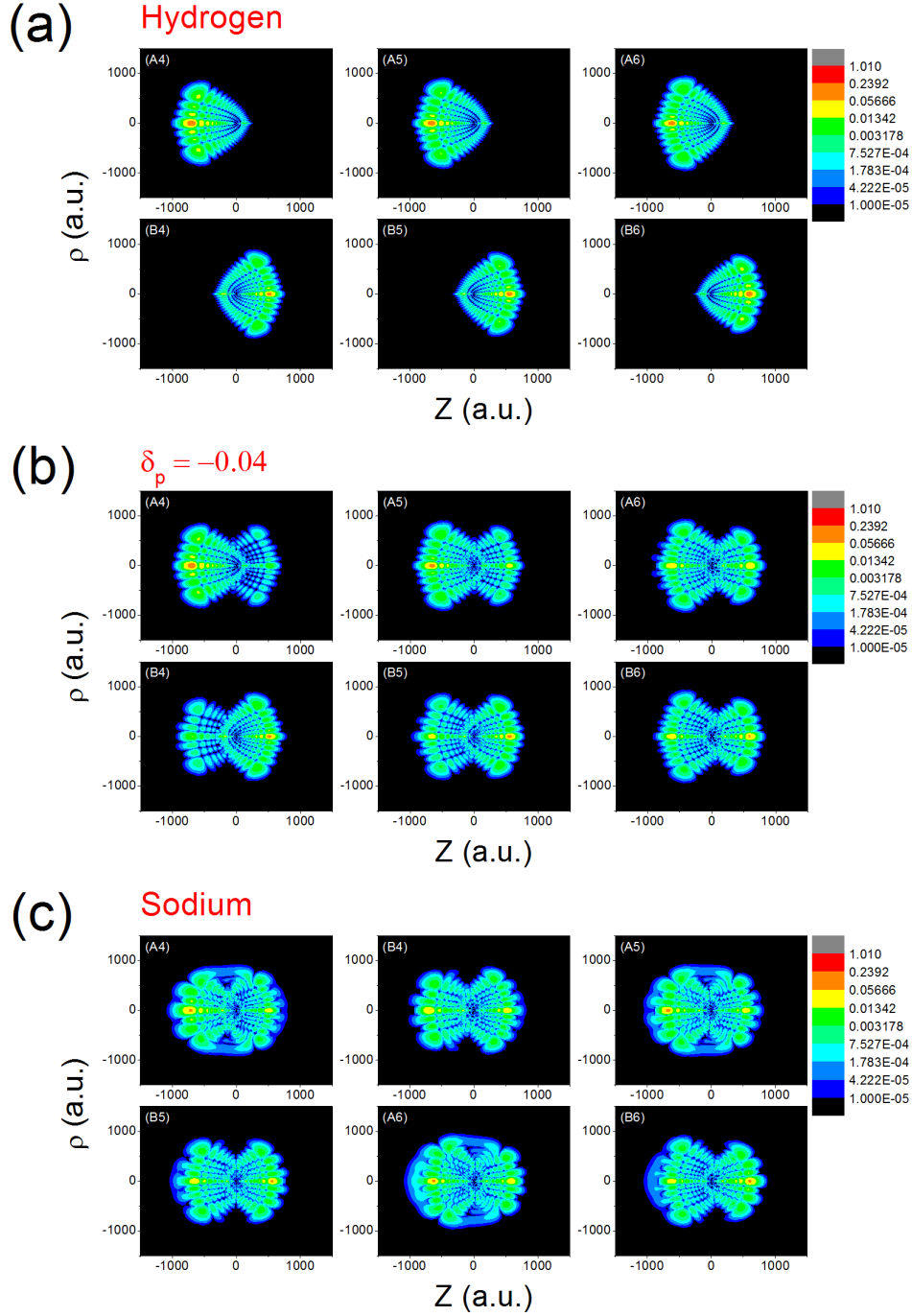


FIG. 3: (Color online) Contour plot of electron probability distribution  $|\Psi(\rho, z)|^2$  for the states marked in Fig.2 for hydrogen (a), artificial atom (b) and sodium (c).

bution  $|\Psi(\rho, z)|^2$  of a parabolic state is localized in area of  $z > 0$  or  $z < 0$ , which depends on whether the state is a blue-shifted state ( $n_1 > n_2$ ) or a red-shifted state ( $n_1 < n_2$ ). This unique feature benefits from the dynamics symmetry of hydrogen atom. There is no combined distribution composed of red and blue states [17]. Unlike hydrogen, however, the electron probability distribution  $|\Psi(\rho, z)|^2$  for artificial atom and sodium loses

this feature [25]. It looks like a superposition of two hydrogenic states at first glance, which clearly shows the core-induced coupling effect in the electron probability distributions. It is shown in Fig. 3(b-c). For example, the probability distribution of both A4 or B4 states of artificial atom can be regarded as a superposition of A4 and B4 states of hydrogen. This point is proved by the numbers of parabola facing towards the negative and pos-



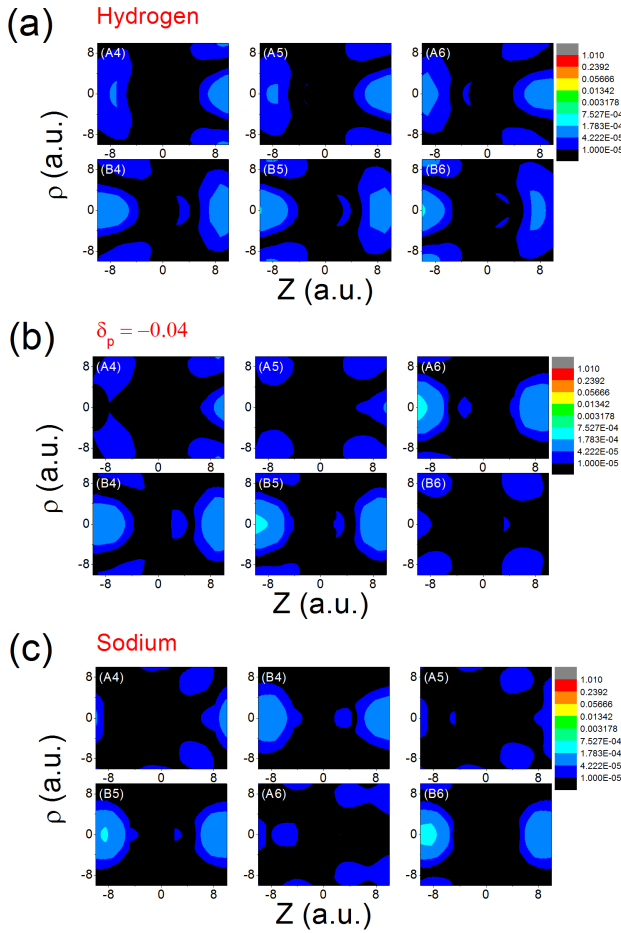


FIG. 4: (Color online) Magnification of Fig.3 for better evaluation of the constructive and destructive interference of wavefunction close to the atomic core. For the  $\pi$  laser irradiation, the initial state has a spindle shape, based on which we can draw a conclusion that the transitions to the states in (a) can have considerable amplitudes since their probability distributions have the same shape. For the non-hydrogenic atoms shown in (b) and (c), however, some states, for example, A4, A5 and B6 in (b) and A4, A5 and A6 in (c), lose the spindle-like distribution, resulting in weak transitions.

itive  $z$ -axis. Obviously, for different state-coupling, the combining weight coefficients are different. Specially, for the coupling scheme A4 shown in Fig.3(b), we can see from the contrast of the probability distribution that the red state is perturbed by the blue state slightly. As its counterpart, seen from B4, the blue state is perturbed by the red state in a small extent. While for sodium, the probability distribution of both A4 or B4 states is not as clear as that for artificial atom shown in Fig.3(b) and it can be viewed as a superposition of more than two red and blue states of hydrogen, which is observable in Fig.3(c).

Since the oscillator strength is proportional to the absolute square of the overlap of the initial state  $\langle i|d$  and the final state  $|f\rangle$  according to the formula given in Eq.6,

we should be able to observe the constructive and destructive interference between red and blue states for the core-induced coupling. As it is known, the ground state of sodium is  $3s^1$ , having a spherical symmetry. The dipole moment term in Eq.6 is proportional to  $\cos\theta$ ,  $d \sim \cos\theta$ , resulting in an initial state with spindle shape. On the other hand, the wavefunction of the ground state is confined in a small radial range, and the final oscillator strength is dependent on the behavior of the final state wavefunction in the same range, where we can also observe the constructive and destructive interference between the red and blue states.

We magnified Fig.3 into Fig.4 to observe the probability distribution close to the nuclear core, within radius less than 10 a.u.. In Fig.4(a), we can see that the probabilities, either for red states A4 to A6 or blue states B4 to B6, have abundant densities along the  $z$ -axis, which sufficiently overlap with the initial state  $\langle i|d$  with spindle shape. All the peaks have close oscillator strengths, in accordance with the given oscillator strengths in Fig.2(a). While for the artificial atom shown in Fig.4(b), only the states of A6, B4 and B5 keep the spindle shape, agreeing with that shown in Fig.2(b). It is caused by the constructive interference between the red and blue states. For the left states A4, A5 and B6, the oscillator strengths are reduced greatly for the destructive interference. As a complex case, for the real atom sodium shown in Fig.4(c), the states B4, B5 and B6 own the spindle shape, giving considerable oscillator strengths, quite consistent with the calculations in Fig.2(c) as well, even for the interactions looking rough and tumble. Anyway, the probability distribution can provide a deeper explanation for the transition intensity based on the conception of constructive or destructive interference between two hydrogenic parabolic states, resulting in enhanced or weakened oscillator strength, respectively.

Mathematically, the final state  $|f\rangle$  can be written as

$$|f\rangle = c_1|red\rangle + c_2|blue\rangle \quad (7)$$

for the simplest case, then the oscillator strength is expressed as

$$\begin{aligned} c_{i \rightarrow f} &= |\langle i|d|f\rangle|^2 \\ &= c_1^2 |\langle i|d|red\rangle|^2 + c_2^2 |\langle i|d|blue\rangle|^2 \\ &\quad + c_1 c_2 \langle i|d|red\rangle^* \langle i|d|blue\rangle + c.c., \end{aligned} \quad (8)$$

where the crossing terms contribute the constructive or destructive interference dependent on the mixing coefficients  $c_1$  and  $c_2$ .

For the higher energy levels, for example, above the stark saddle point  $E_c$ , as shown in Fig.5, more states come to interact with each other, leading to more complex oscillator re-distributions. For hydrogen atom, as can be seen from Fig.5(a), the oscillator strength distribution above  $E_c$  still shows regularity like the states below the saddle point  $E_c$ . For non-hydrogenic atoms, however, the core-induced interaction causes the oscillator strength to behave chaotic

TABLE II: The energy level positions (in  $\text{cm}^{-1}$ ) of the stark resonances of hydrogen and sodium ( $F = 840 \text{ V/cm}$ ,  $m = 0$ ) within  $-175 \text{ cm}^{-1} \sim -145 \text{ cm}^{-1}$  corresponding to the transitions in Fig.5.

State:( $n_1, n_2, m$ )	hydrogen		sodium	
	Theory <sup>a</sup>	Theory <sup>b</sup>	Theory <sup>c</sup>	Experiment <sup>d</sup>
(20,3,0)	-169.589	-169.589	-169.319	-169.320
(21,2,0)	-166.972	-166.971	-167.172	-167.054
(22,1,0)	-164.352	-164.351	-164.378	-164.113
(23,0,0)	-161.729	-161.729	-161.599	-161.348
(20,4,0)	-155.388	-155.388	-155.289	-155.289
(21,3,0)	-152.655	-152.655	-152.778	-152.366
(22,2,0)	-149.920	-149.920	-149.954	-149.718
(23,1,0)	-147.181	-147.181	-147.131	-147.036
(24,0,0)	-144.440	-144.440	-144.592	-144.592
(2,27,0)	-168.273	-168.735	-168.710	-168.710

<sup>a</sup> Calculation for hydrogen by the seventh-order perturbation theory [8];

<sup>b</sup> Calculation for hydrogen by the present EQDT method;

<sup>c</sup> Calculation for sodium by the present EQDT method;

<sup>d</sup> Experimental observation for sodium with total Gaussian broadening of  $0.18 \text{ cm}^{-1}$ .

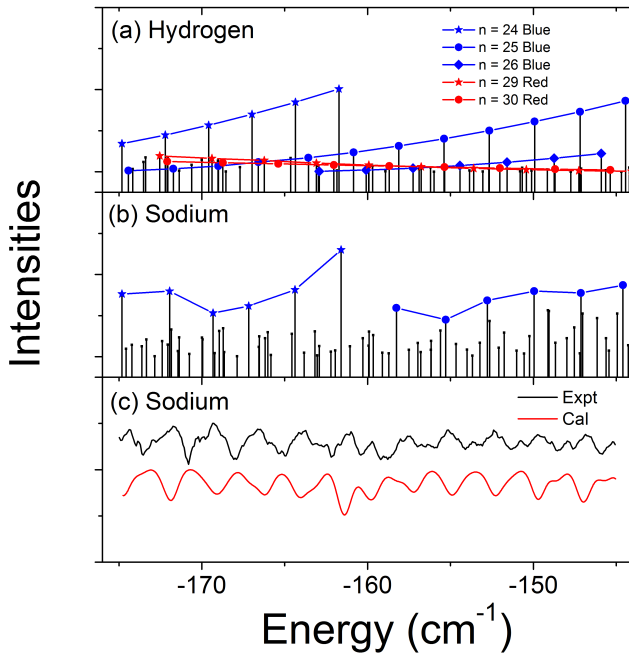


FIG. 5: (Color online) Calculated oscillator strength above the saddle point  $E_{sp} = -177.4 \text{ cm}^{-1}$  at  $F = 840 \text{ V/cm}$  for (a) hydrogen atom, (b) sodium atom. The calculate spectral lines are convoluted with a Gaussian broadening and compared with the experimental observations as well (c).

completely as shown in Fig.5(b) although the broadened experimental spectrum shows a smooth oscillation in Fig.5(c). The oscillation spacing in our spectrum,  $2.67 \text{ cm}^{-1}$ , is very close to the estimation by formula  $3\epsilon n_c a_0 \simeq (9.16 \text{ cm}^{-1})(\epsilon/4335 \text{ V/cm})^{3/4}$  [37], which

gives a value of  $2.68 \text{ cm}^{-1}$  at electric field of  $840 \text{ V/cm}$ .

However, the energy levels above  $E_c$  have a different feature compared with those below  $E_c$ , that is, the red states above saddle point have very short lifetime, making the spectral lines extremely broadened. Like table I, we also give the energy level positions for hydrogen and sodium in table II. Similar to the case below  $E_c$ , we draw the electron probability distributions for several typical states given in Fig.5. They are shown in Fig.6. It's worth noting that the red states above  $E_c$  have extremely short lifetime, but their coupling with blue states will prolong their lifetime greatly, providing a chance to perform 'photoionization microscopy' [25]. In Fig.6(a), the resonant state of sodium at  $E = -155.289$  can be viewed as the superposition of the hydrogen parabolic states (6, 23) and (20, 4). Specially, we give a state of sodium with decomposition of one red and two blue states, which is shown in Fig.6(b). Obviously, the blue state (15, 9) contributes the least for the final sodium state at  $E = -169.32$ . For all the above cases, however, the components of red or blue states will come to interference close to the atomic core.

#### IV. CONCLUSION

In summary, we demonstrate that the electric-field-induced coupling can be clearly visualized in the form of wave-functions. The parabolic separation for hydrogen in electric field can supply a set of 'orthogonal' basis composed of red and blue states and the non-hydrogenic behaviour of Rydberg sodium in electric field can be seen as coupling between hydrogenic red and blue states. By viewing the electron probability distributions directly, we

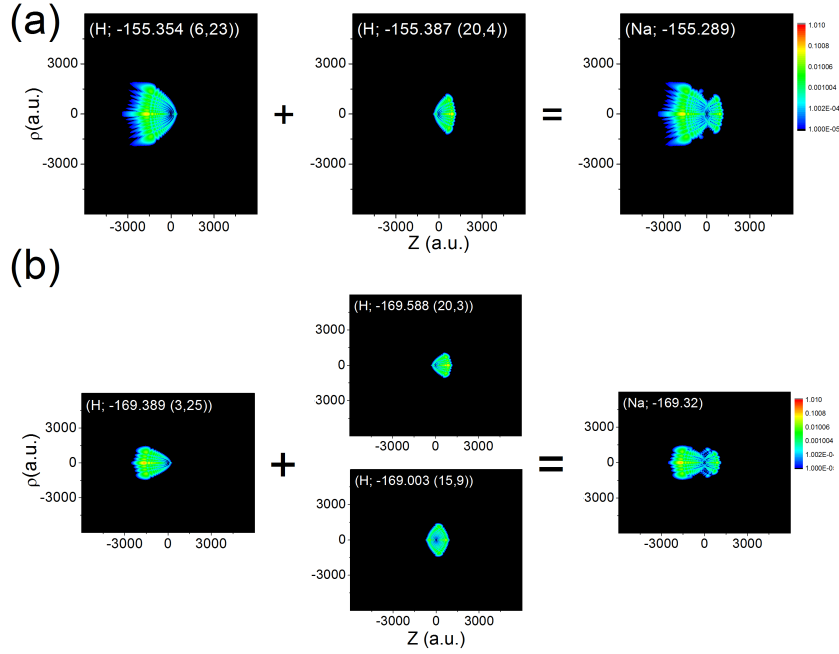


FIG. 6: (Color online) Contour plot of electron probability distribution  $|\Psi(\rho, z)|^2$  for some typical states in Fig. 5. Each state of sodium can be considered as a superposition of two or more hydrogenic parabolic states.

show that the non-hydrogenic wave-function can be intuitive in understanding the coupling behaviour of non-hydrogenic atom in static electric fields on benefit of the ‘orthogonality’ of basis. Moreover, the irregular oscillator strength distribution of sodium is analyzed in the perspective of electric-field-induced interference between hydrogenic red and blue states. The constructive and destructive interferences are confirmed in the wavefunction analysis and well explain the oscillator strength from theoretical calculation and experimental observation for Rydberg sodium in electric field of 840 V/cm.

#### Acknowledgments

This work was supported by the National Basic Research Program of China under grant No. 2013CB922003, by the National Natural Science Foundation of China under grant Nos. 11174329, 91121005 and 91421305.

- 
- [1] M. L. Zimmerman, M. G. Littman, M. M. Kash, and D. Kleppner, *Phys. Rev. A* **20**, 2251 (1979).
  - [2] D. A. Harmin, *Phys. Rev. A* **26**, 2656 (1982).
  - [3] D. A. Harmin, *Phys. Rev. Lett.* **49**, 128 (1982).
  - [4] M. Courtney, N. Spellmeyer, H. Jiao, and D. Kleppner, *Phys. Rev. A* **51**, 3604 (1995).
  - [5] J. A. West and J. Stroud, C. R., *Opt. Express* **1**, 31 (1997).
  - [6] T. F. Gallagher, L. M. Humphrey, W. E. Cooke, R. M. Hill, and S. A. Edelstein, *Phys. Rev. A* **16**, 1098 (1977).
  - [7] M. G. Littman, M. M. Kash, and D. Kleppner, *Phys. Rev. Lett.* **41**, 103 (1978).
  - [8] H. Silverstone, *Phys. Rev. A* **18**, 1853 (1978).
  - [9] J. Gao, J. B. Delos, and M. Baruch, *Phys. Rev. A* **46**, 1449 (1992).
  - [10] J. Gao and J. B. Delos, *Phys. Rev. A* **46**, 1455 (1992).
  - [11] J. Xi, X. He, and B. Li, *Phys. Rev. A* **46**, 5806 (1992).
  - [12] A. R. Edmonds, *J. Phys. B* **6**, 1603 (1973).
  - [13] Y. Li, W. Y. Liu, and B. W. Li, *J. Phys. B* **29**, 1433 (1996).
  - [14] J. M. Menéndez, I. Martín, and A. M. Velasco, *J. Chem. Phys.* **119**, 12926 (2003).
  - [15] V. D. Kondratovich and V. N. Ostrovsky, *J. Phys. B* **17**, 2011 (1984).
  - [16] V. D. Kondratovich and V. N. Ostrovsky, *J. Phys. B* **23**, 3785 (1990).
  - [17] A. S. Stodolna, A. Rouzée, F. Lépine, S. Cohen, F. Robicheaux, A. Gijsbertsen, J. H. Jungmann, C. Bordas, and M. J. J. Vrakking, *Phys. Rev. Lett.* **110**, 213001 (2013).
  - [18] A. T. J. B. Eppink and D. H. Parker, *Rev. Sci. Instrum.* **68**, 3477 (1997).
  - [19] H. L. Offerhaus, C. Nicole, F. Lépine, C. Bordas, F. Rosca-Pruna, and M. J. J. Vrakking, *Rev. Sci. Instrum.* **72**, 3245 (2001).
  - [20] L. B. Zhao and J. B. Delos,



- Phys. Rev. A* **81**, 053418 (2010).
- [21] L. B. Zhao and J. B. Delos, *Phys. Rev. A* **81**, 053417 (2010).
- [22] D. A. Harmin, *Phys. Rev. A* **24**, 2491 (1981).
- [23] F. Robicheaux and J. Shaw, *Phys. Rev. A* **56**, 278 (1997).
- [24] L. B. Zhao, I. I. Fabrikant, J. B. Delos, F. Lpine, S. Cohen, and C. Bordas, *Phys. Rev. A* **85**, 053421 (2012).
- [25] A. S. Stodolna, F. Lépine, T. Bergeman, F. Robicheaux, A. Gijssbertsen, J. H. Jungmann, C. Bordas, and M. J. J. Vrakking, *Phys. Rev. Lett.* **113**, 103002 (2014).
- [26] J. Y. Liu, P. McNicholl, D. A. Harmin, J. Ivri, T. Bergeman, and H. J. Metcalf, *Phys. Rev. Lett.* **55**, 189 (1985).
- [27] W. Gao, H. F. Yang, H. Cheng, X. J. Liu, and H. P. Liu, *Phys. Rev. A* **86**, 012517 (2012).
- [28] H. F. Yang, W. Gao, H. Cheng, and H. P. Liu, *Phys. Scr.* **87**, 035301 (2013).
- [29] I. Seipp and K. T. Taylor, *J. Phys. B* **27**, 2785 (1994).
- [30] I. Martin, A. Lavin, M. Karwowski, and J. Karwowski, *Chem. Phys. Lett.* **255**, 89 (1996).
- [31] M. Inmaculada, K. Jacek, L. Carmen, and H. F. D. Geerd, *Phys. Scr.* **44**, 567 (1991).
- [32] H. Bachau, E. Cormier, P. Decleva, J. E. Hansen, and F. Martn, *Rep. Prog. Phys.* **64**, 1815 (2001).
- [33] J. G. Rao, W. Y. Liu, and B. W. Li, *Phys. Rev. A* **50**, 1916 (1994).
- [34] D. Delande, A. Bommier, and J. C. Gay, *Phys. Rev. Lett.* **66**, 141 (1991).
- [35] V. Kondratovich and J. B. Delos, *Phys. Rev. A* **56**, R5 (1997).
- [36] J. W. B. Hughes, *Proc. Phys. Soc.* **91**, 810 (1967).
- [37] A. R. P. Rau and K. T. Lu, *Phys. Rev. A* **21**, 1057 (1980).